# Temperature-dependent impact of non-PAN peroxy nitrate formation, $RO_2NO_2$, on nighttime atmospheric chemistry[†]

*– Supporting information –*

Michelle Färber, Luc Vereecken, Hendrik Fuchs, Georgios I. Gkatzelis, Franz Rohrer, Sergej Wedel, Andreas Wahner, and Anna Novelli

## Contents

# A Investigation of the ozonolysis of trans-2-hexene

The FZJ mechanism includes among other modifications an updated ozonolysis and isomerisation scheme compared to the MCM (Section 2.3). Since ozonolysis also contributes to the nighttime chemistry (Tab. S3) the validity of this mechanism was separately tested with an ozonolysis experiment with trans-2-hexene ($T \approx 280$ K).

Measured species are compared with model results using either the FZJ mechanism or

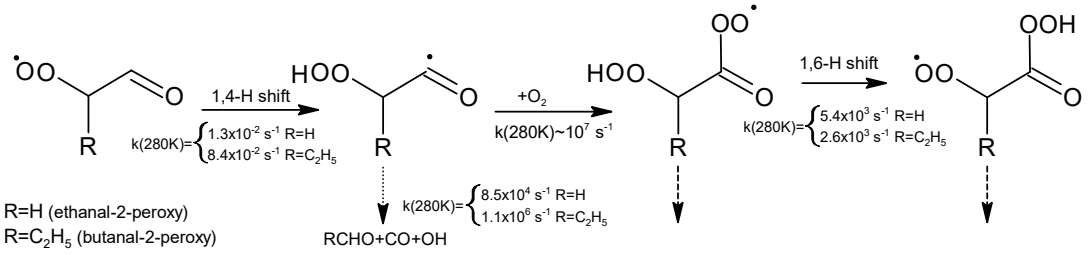


Figure S1: Generalised isomerisation scheme of ethanal-2-peroxy and butanal-2-peroxy based on quantum mechanical calculations by Novelli *et al.* [1]. Dashed lines indicate the loss of $RO_2$ through reaction with NO, $NO_2$, $HO_2$, and R'$O_2$, while dotted lines display decomposition reactions.

the MCM. The measured time series of trans-2-hexene and ozone are very well described by all mechanisms within the uncertainties (Fig. S2). Measured $HO_2$ radical concentrations agree with the MCM and FZJ mechanisms within 20 % and 30 %, respectively. Predicted $HO_2$ radical concentrations are similar for all models; the $HO_2$ production is predominantly driven by the OH + CO reaction, contributing to about 83 % to the total $HO_2$ production, while $HO_2$ is lost via its reactions with $RO_2$ and $O_3$, contributing to about 50 % and 35 % to the total $HO_2$ loss, respectively.

For the MCM mechanism, a model-to-measurement ratio of up to 2.8 is found for $RO_2$ radicals formed. In comparison, the FZJ mechanism substantially improves the agreement (agreement within 27 % on average, and a maximum deviation of a factor 1.7), since less $RO_2$ are expected to be formed in the FZJ mechanism than in the MCM due to a lower $RO_2$ yield from ozonolysis (59 % in the FZJ mechanism, 70 % in the MCM). However, modelled $RO_2$ radical concentrations remain up to a factor of 1.7 higher than measured values, particularly after the first injection. This was also observed by Novelli *et al.* [1] for $RO_2$ formed in the nighttime oxidation of trans-2-hexene when ozonolysis dominated the chemistry.

For this reason, the isomerisation scheme (Fig. S1) of the $RO_2$ radicals from the ozonolysis, ethanal-2-peroxy and butanal-2-peroxy, was tested separately by comparing model results when their isomerisation reactions are included or not (Figs. S2 and S3). The impact of the isomerisation of ethanal-2-peroxy and butanal-2-peroxy on the total $RO_2$ is small, and results from the models with and without $RO_2$ isomerisation reactions agree within 10 % (Fig. S2). However, including isomerisation reactions does influence the $RO_2$ speciation, displayed in Fig. S3. While the FZJ mechanisms yield similar contributions of methyl and propyl peroxy radical concentrations to the total $RO_2$ radical concentration (approximately 36 % combined), differences emerge in the allocation of the remaining $RO_2$ species. In the FZJ model without $RO_2$ isomerisation, these $RO_2$ are distributed among oxygenated peroxy radicals like ethanal-2-peroxy and butanal-2-peroxy. In contrast, in the FZJ model including $RO_2$ isomerisation, they are apportioned between their respective isomerisation products, ethyl-1-peracid-2-peroxy and butyl-1-peracid-2-peroxy, with a minor contribution from ethanal-2-peroxy and butanal-2-peroxy. Due to

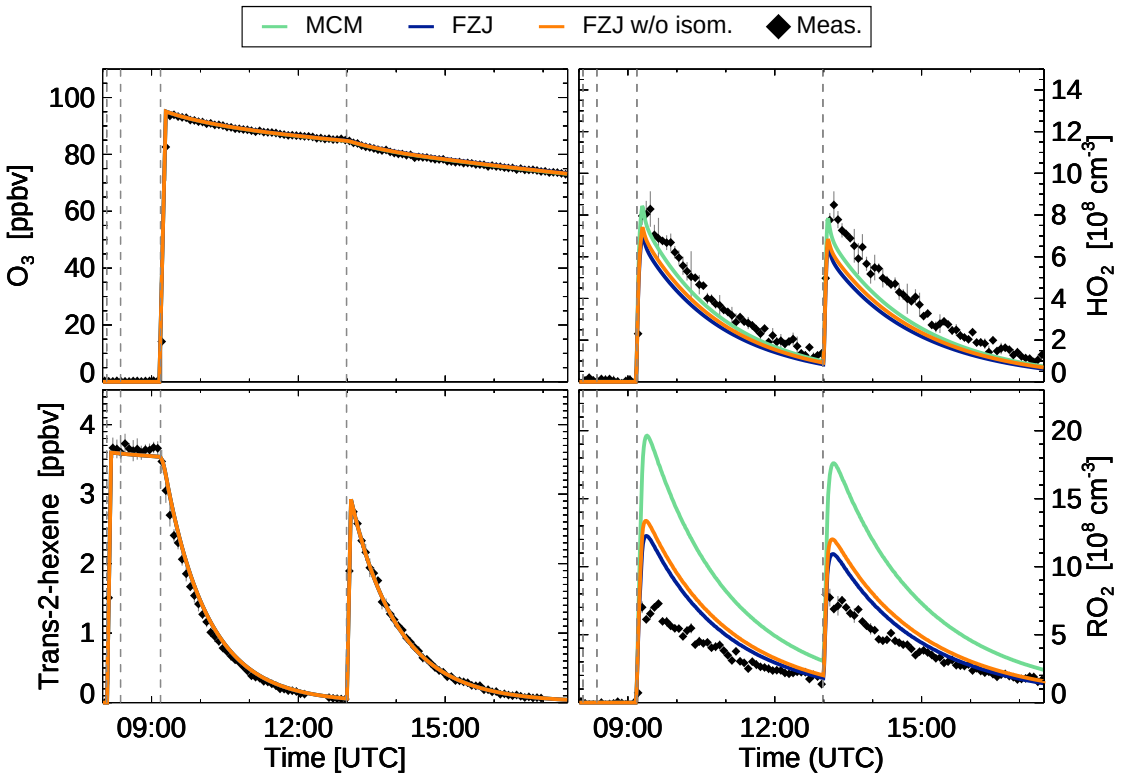


Figure S2: Comparison between modelled and measured (5 minutes average) trace gases and $HO_2$ and $RO_2$ radical concentrations for three different mechanisms for the ozonolysis experiment of trans-2-hexene at 280 K. Model results displayed as FZJ and FZJ w/o isom models refer to the FZJ mechanism with and without $RO_2$ isomerisation reactions, respectively. Injections of chemical species into the chamber are marked by vertical lines.

similar lifetimes of all these $RO_2$, the total $RO_2$ radical concentration does not significantly change whether isomerisation reactions are included in the model or not. Measurements of speciated $RO_2$ would be necessary to validate the isomerisation scheme.

An updated ozonolysis scheme following the recent recommendation by Newland *et al.*[2] was also tested. In short, the main difference comprises a yield of 40 % towards the $C_3$ carbonyl compounds as compared to 50 % as used in this study. The major impact is on the modelled acetaldehyde (increase of $\sim$ 40 % as compared to the FZJ mechanism) with negligible differences for the radicals. To bring measured and modelled $RO_2$ radicals in agreement a total yield of $RO_2$ as low as $\sim$ 20 % would be needed. Although there is a lack of studies focusing directly on trans-2-hexene ozonolysis, this would be in stark disagreement with the molecules used to develope the SAR (1 and 3-hexene).

In the following, the remaining discrepancy between modelled and measured $RO_2$ is further discussed, examining the potential impact of the peracidic functionality on the $RO_2$ chemistry and detection. A partial detection of $RO_2$ by the FZJ-$RO_x$LIF instrument due to the formation of organic nitrites (RONO) or carbonyl compounds (RC=O) in the reaction of RO with NO can be excluded. Table S1 shows pseudo-first order loss rates of the main RO radicals in the ozonolysis reaction with trans-2-hexene. For all listed RO radicals, the reaction of RO with NO does not compete with the other RO loss reactions. The fate of the peracid-substituted $RO_2$ radicals was mostly estimated from the SAR in Jenkin *et al.*[3], which does not consider peracid substituents explicitly. Due to the large contribution of peracidic peroxy radicals to the total $RO_2$ the modelled total $RO_2$ is sensitive to their

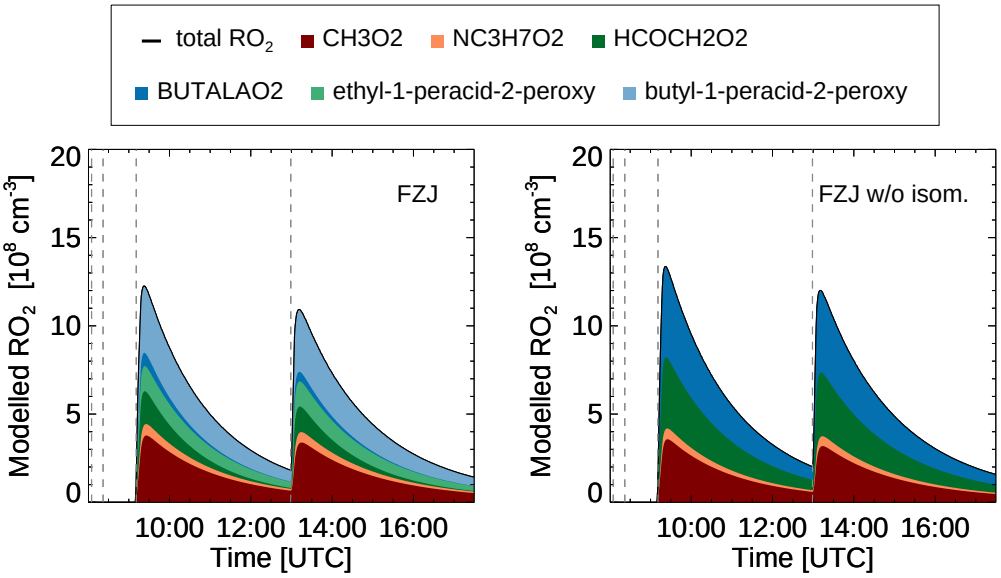


Figure S3: Model results of time-dependent speciation of $RO_2$ radicals obtained for the FZJ mechanism with (FZJ) and without (FZJ w/o isom) $RO_2$ isomerisation reactions. Contributions of butanal-2-peroxy, ethanal-2-peroxy, and the $RO_2$ formed subsequently their isomerisation are shown. Injections of chemical species into the chamber are marked by vertical lines.

chemistry (Fig. S4).

Removing the fraction of $RO_2$ stored in form of butyl-1-peracid-2-peroxy from the observable $RO_2$ would improve the agreement between modelled and measured $RO_2$ significantly (model-to-measurement ratio improved from 1.38 to 0.92 for the first injection period), but the exclusion of both, ethyl-1-peracid-2-peroxy and butyl-1-peracid-2-peroxy, would result in an underestimation of the measured $RO_2$ (model-to-measurement ratio of 0.7 for the first injection period). This observation is consistent with the systematic study performed by Novelli *et al.*[1] who observed a good agreement between measured and modelled (FZJ model) nighttime $RO_2$ for cis-2-butene but a discrepancy for 1-pentene and trans-2-hexene. While only ethanal-2-peroxy and thus ethyl-1-peracid-2-peroxy are formed in the ozonolysis of cis-2-butene, butanal-2-peroxy and thus butyl-1-peracid-2-peroxy are predicted for 1-pentene and trans-2-hexene. The presence of an alkyl moiety may have an impact on the respective $RO_2$ chemistry that we are currently not aware of. However, as we are lacking speciated $RO_2$ measurements in this work, we cannot unam-

Table S1: Comparison of the pseudo-first order loss rates of main RO radicals formed in the ozonolysis of trans-2-hexene. The loss rates were determined for conditions present inside the FZJ-RO$_x$LIF reactor ($\sim 25$ hPa, $\sim 3 \times 10^{11}$ cm$^{-3}$ of NO, 6 s residence time). $k_{dec}$ and $k_{isom}$ refer to unimolecular reaction rate coefficients for the decomposition and isomerisation of RO radicals, respectively. Rate coefficients for the bimolecular reactions of RO with $O_2$ (H abstraction reaction) and with NO are denoted as $k_{\mathrm{H}abstr}$ and $k_{\mathrm{RO+NO}}$, respectively.

| RO radical | $k_{dec}$ [s$^{-1}$] | $k_{isom}$ [s$^{-1}$] | $k_{\mathrm{H}abstr} \cdot [\mathrm{O_2}]$ [s$^{-1}$] | $k_{\mathrm{RO+NO}} \cdot [\mathrm{NO}]$ [s$^{-1}$] |
|---|---|---|---|---|
| $CH_3O^\bullet$ | | | 183 | 4 |
| $C_2H_5CH(OH)C(=O)O^\bullet$ | $5.3 \times 10^{12}$ | | | 14 |
| $CH_2(O^\bullet)C(=O)OOH$ | 0.6 | $2.8 \times 10^3$ | $1.1 \times 10^3$ | 14 |

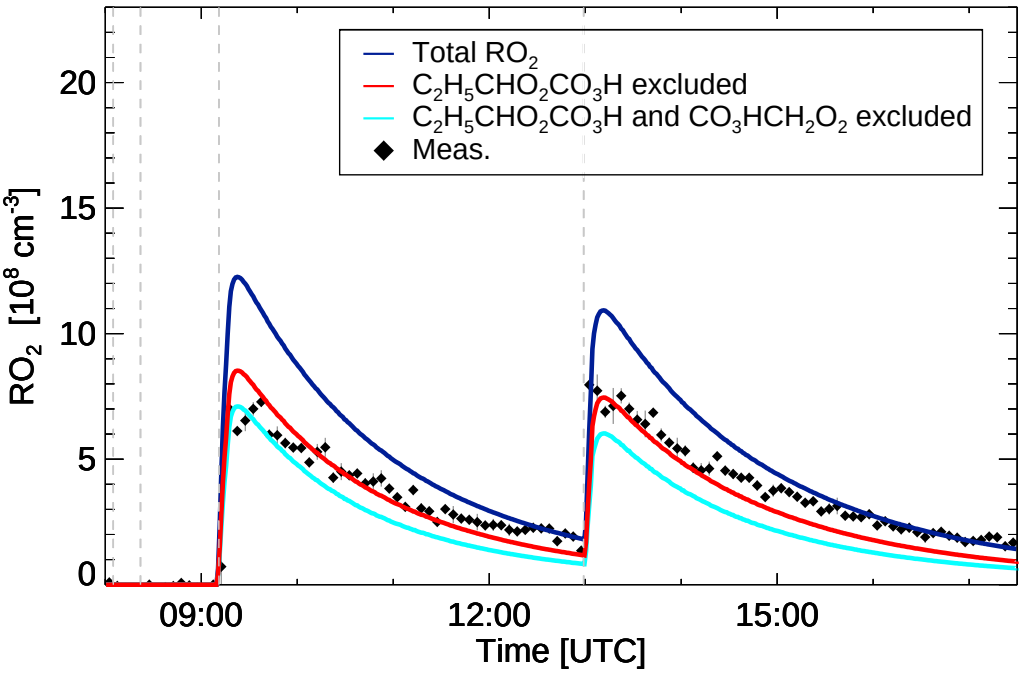


Figure S4: Comparison of modelled and measured (5 minutes average) total $RO_2$ concentrations in the ozonolysis experiment of trans-2-hexene. Model results are based on the FZJ mechanism. Displayed modelled $RO_2$ show the total $RO_2$ and total $RO_2$ excluding either butyl-1-peracid-2-peroxy or ethyl-1-peracid-2-peroxy and butyl-1-peracid-2-peroxy.

biguously decide which $RO_2$ is aberrant, making speculations on the exact nature of the missing chemistry complex.

For the nighttime trans-2-hexene experiments, ozonolysis is contributing most in the experiment performed at low temperatures ($T \approx 276$ K), but less so for the higher temperatures (Tab. S3). Figure S5 shows total $RO_2$ modelled by the FZJ mechanism including non-acyl $RO_2NO_2$ formation, but with and without including butyl-1-peracid-2-peroxy in the observable $RO_2$. For hot and medium temperatures, the modelled total $RO_2$ improves somewhat when ignoring the contribution of butyl-1-peracid-2-peroxy, however, for cold conditions, measured $RO_2$ radical concentrations are now underestimated by a factor of 1.5. Such behaviour could be consistent with a loss process that is temperature dependent and becomes less important at lower temperatures, *e.g.* a unimolecular reaction of butyl-1-peracid-2-peroxy not forming a new $RO_2$ radical. However, some unimolecular reactions have been considered by Novelli *et al.* [1], and none are competitive. Simulations adding dummy bimolecular reactions with the typical co-reactants, $HO_2$ and $RO_2$, likewise did not suggest any suitable pathways.

Overall, at the present time the cause for the $RO_2$ discrepancy observed in the ozonolysis experiment remains unknown. Further investigations of the $RO_2$ chemistry of peracid

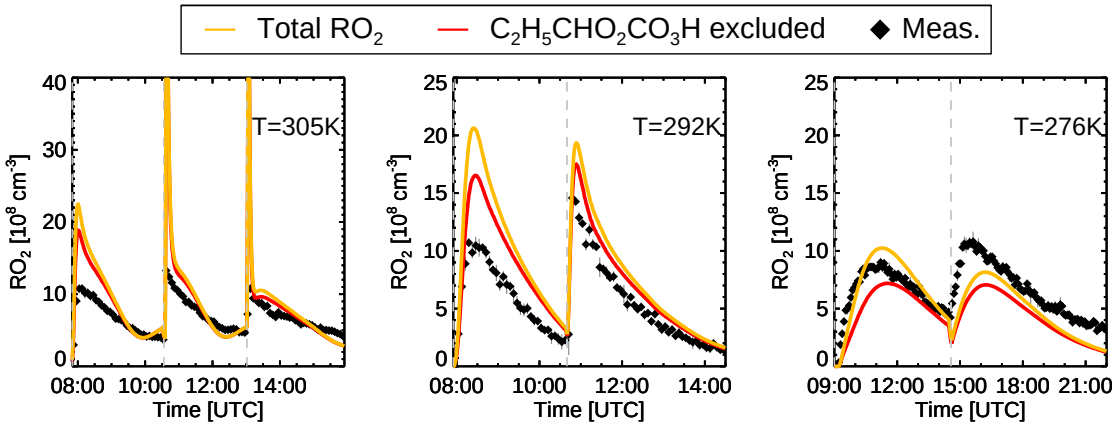


Figure S5: Comparison of modelled and measured (5 minutes average) total $RO_2$ concentrations for the nighttime experiments of trans-2-hexene. Model results are based on the FZJ mechanism including additional formation of non-acyl $RO_2NO_2$. Displayed modelled $RO_2$ show the total $RO_2$ and total $RO_2$ excluding butyl-1-peracid-2-peroxy.

peroxy radicals would be required as well as measurements of speciated $RO_2$. Important, though, is that the impact of the discrepancy in the ozonolysis chemistry remains rather limited in the nighttime experiments (Fig. S5), such that the main conclusions on the impact of peroxynitrate formation are robust against the uncertainties on the fate of butyl-1-peracid-2-peroxy.

## B Estimation of the $NO_3$ interference in the $RO_x$ system

In the $NO_3$-oxidation experiment of trans-2-hexene at high temperatures, a $NO_3$ interference was observed in the $RO_x$ cell. The $RO_x$ system of the LIF instrument is run in two modes, with and without addition of NO in the converter, enabling the measurement of $RO_x$ (= OH + $HO_2$ + $RO_2$) or $HO_2(RO_x)$ (= $HO_2$ + interfering $RO_2$), respectively. $HO_2(RO_x)$ is not further evaluated but it can be used as an indicator for possible interferences. If no interference is present, the following is valid:

$$HO_2(RO_x) \leq RO_x. \tag{S1}$$

The two observables are shown in Fig. S6, together with the modelled $NO_3$ mixing ratio for the aforementioned experiment of interest. For $NO_3 \gtrapprox 20$ pptv, $HO_2(RO_x)$ starts to deviate from $RO_x$ such that Eq. (S1) no longer holds. As there is no evidence for a change

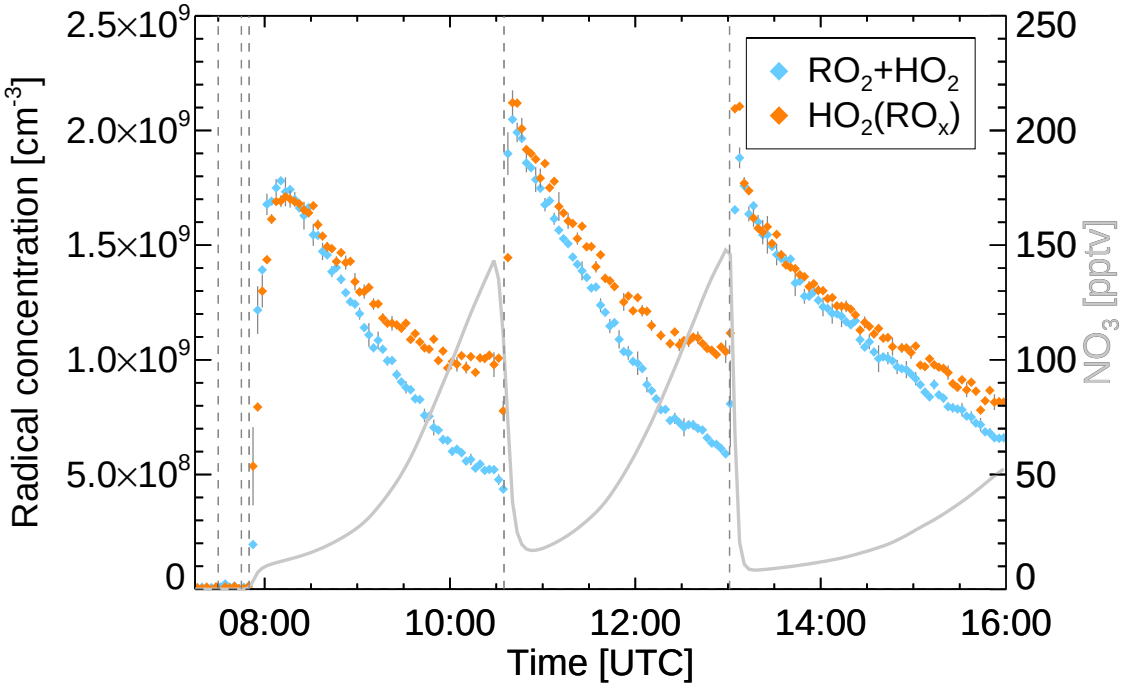


Figure S6: Comparison between $RO_x$ and $HO_2(RO_x)$ radical concentrations, measured with the $RO_x$LIF radical instrument (3 minutes average) in the nighttime oxidation of trans-2-hexene at hot conditions. Injections of chemical species into the chamber are marked by vertical lines.

in the sensitivity of the instrument between the two modes, this discrepancy can only be explained by an interference. A lower limit of the interference signal in the $RO_x$ system, without adding NO in the converter, is given by the difference of $HO_2(RO_x)$ and $RO_x$ since it is assumed that all $RO_2$ are converted to OH or $HO_2$ in the $RO_x$ detection cell. According to Fuchs *et al.*[4], the interference signal in the $RO_x$ system, when adding NO in the converter, is two times smaller, therefore, it can be treated as an estimate for the $NO_3$ interference in the $RO_x$ measurement.

By performing a linear regression, a $NO_3$ interference of $3.6 \times 10^6\,\mathrm{cm}^{-3}$ per pptv of

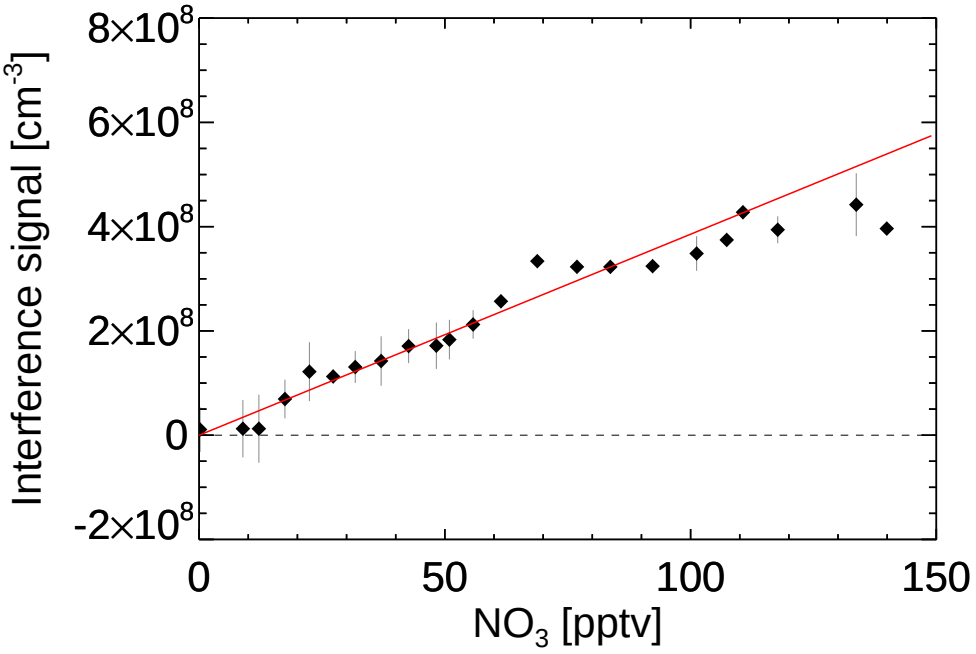


Figure S7: Correlation plot of the estimated $NO_3$ interference. The interference signal is derived from the difference of $HO_2RO_x$ and the sum of $HO_2$ and $RO_2$ radicals.

$NO_3$ could be estimated (see Fig. S7). Figures S8 and S9 display the impact of the $NO_3$ interference on the measured $HO_2$ and $RO_2$ radical concentrations. Overall, the $NO_3$ interference in the $RO_2$ radical measurement only affects the trans-2-hexene experiment at high temperatures where the interference decreases the $RO_2$ by approximately a factor of 1.5.

The $NO_3$ interference in the $HO_2$ radical measurement could not be determined in this study, therefore, a recently reported value for the previous SAPHIR-$RO_x$LIF system of $1 \times 10^6$ cm$^{-3}$ per pptv $NO_3$ was taken from Fuchs *et al.*[4]. Corresponding interference-corrected $HO_2$ radical concentrations are lowered by $\approx 25$ % relative to the measured $HO_2$ for the trans-2-hexene experiment at high temperatures (Fig. S8). Similarly to $RO_2$, the $NO_3$ interference in the $HO_2$ radical measurement is only important for hot conditions, therefore it is not considered for the remaining experiments. For the experiment at high temperatures, the interference is taken into account in the mechanisms by adding it to the modelled $HO_2$ and $RO_2$ radicals.

For the cis-2-butene experiments, including the $NO_3$ interference does not affect the $HO_2$ and $RO_2$ radical.

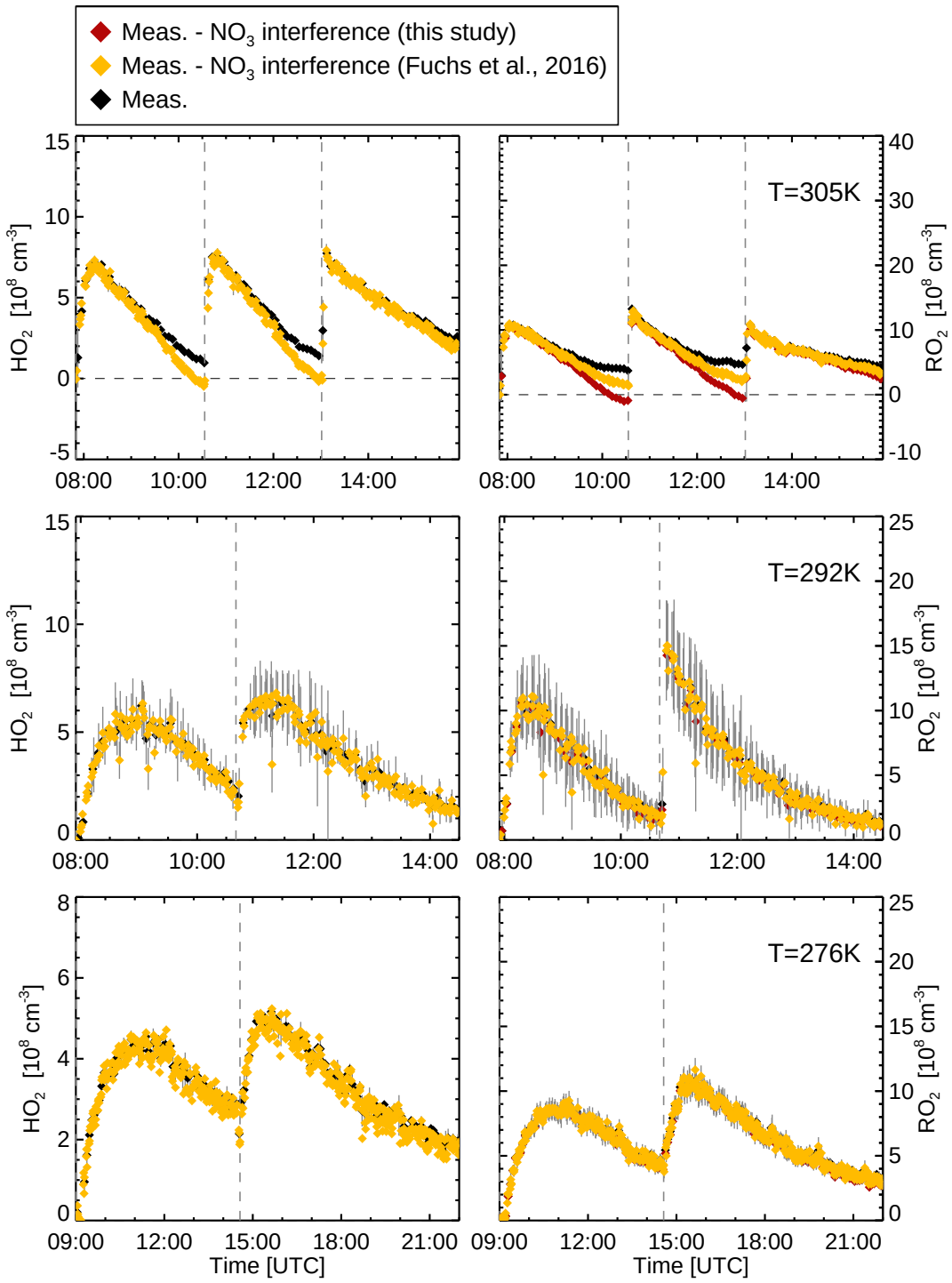


Figure S8: Measured (5 minutes average) $HO_2$ and $RO_2$ radical concentrations in the trans-2-hexene experiments at cold, medium, and hot temperatures, with and without including the $NO_3$ interference, derived from this work for $RO_2$ and taken from Fuchs *et al.*[4] for $HO_2$. Injections of chemical species into the chamber are marked by vertical lines.

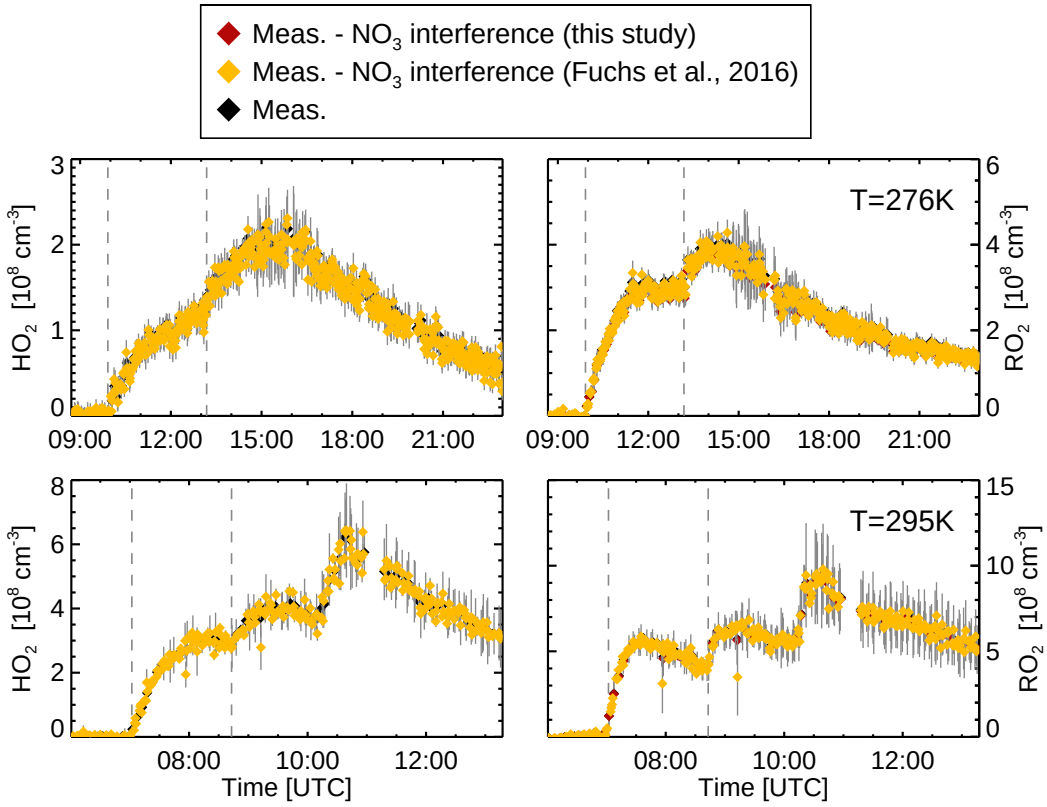


Figure S9: Measured (5 minutes average) $HO_2$ and $RO_2$ radical concentrations in the cis-2-butene experiment at cold and medium temperatures, with and without the $NO_3$ interference, derived from this work for $RO_2$ and taken from Fuchs *et al.*[4] for $HO_2$. Injections of chemical species into the chamber are marked by vertical lines.

## C Modified $CH_3CH(NO_3)CH(CH_3)O$ decomposition rate

A previous study on β-nitrate alkoxy radicals by Novelli *et al.*[1] showed that specific β-nitrate alkoxy radicals, >C($ONO_2$)C($O^\bullet$)<, decompose with a rate of about $4.5 \times 10^4\ s^{-1}$ at 298 K. The reaction with $O_2$ or isomerisation are not competitive in the $RO_x$ converter at room temperature. Since the $RO_2$ detection relies on the formation of OH or $HO_2$ in the

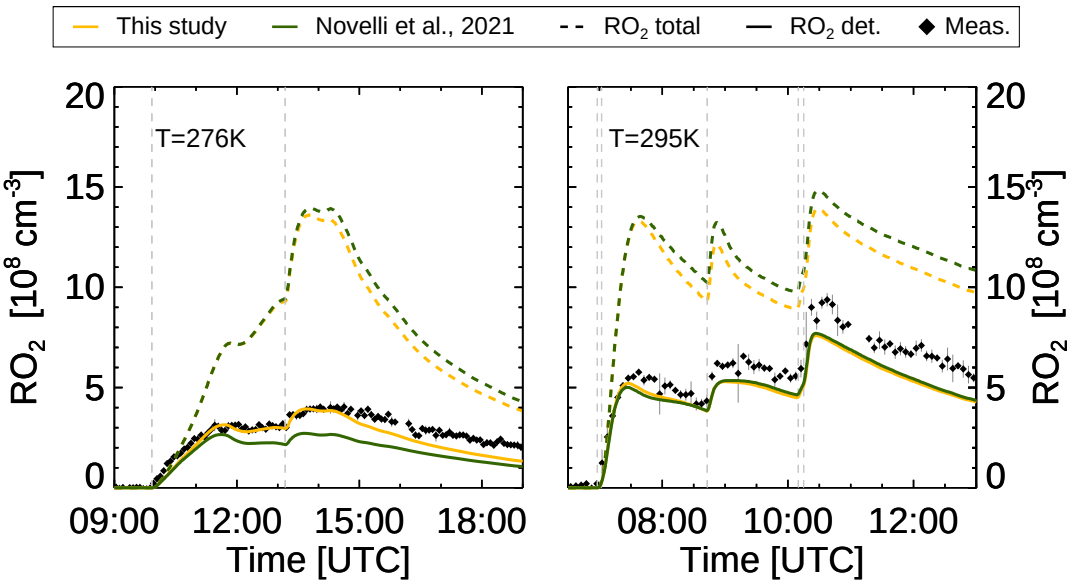


Figure S10: Comparison of modelled time series with measurements for the decomposition rates of $CH_3CH(NO_3)CH(CH_3)O$ (MCM notation: C42NO33O) used by Novelli *et al.*[1] (Eq. (S2)) and in this work (Eq. (S3)) for the cis-2-butene experiments. Model results are based on the FZJ mechanism including additional formation of non-acyl $RO_2NO_2$. Injections of chemical species into the chamber are marked by vertical lines.

process of the reaction of $RO_2$ with NO, the detectability of the according peroxy radical $CH_3CH(OO^\bullet)CH(ONO_2)CH_3$ (MCM notation: C42NO33O2) is affected.
The decomposition rate of $CH_3CH(NO_3)CH(CH_3)O$ (MCM notation: C42NO33O) was calculated theoretically in the study by Novelli *et al.*[1] and was modified within its uncertainty to improve the agreement between model and measurement for cold conditions. Figure S10 displays the comparison of the modelled $RO_2$ radical concentrations with the decomposition rate as used in the study by Novelli *et al.*[1] and with the new one:

$$k_{dec}|_{\text{Novelli } et\ al.} = 2.94 \times 10^9 \cdot T^{1.32} \times \exp\left(-\frac{5542}{T}\right), \tag{S2}$$

$$k_{dec}|_{\text{this study}} = 2.94 \times 10^9 \cdot T^{1.32} \times \exp\left(-\frac{5860}{T}\right). \tag{S3}$$

In the tested temperature range (from 276 K to 305 K), the decomposition rate, used in this work, is deviating by maximum a factor of 3 from the decomposition rate used by Novelli *et al.*[1]. This is on the higher end of the expected uncertainty (factor of 2 to 3) of the theoretically calculated rate in Novelli *et al.*[1], but remains comparable to the variability between the various stereo-specific $RO_2$ isomers and the uncertainty on the rate

predictions.
The decomposition rate, as used in this study, results in a detectability of 16 % at 279 K (increasing from 5 % with the decomposition rate from Novelli *et al.*[1]) and of 5 % at 295 K (increasing from 1.7 % with the decomposition rate from Novelli *et al.*[1]).
For the analogous $CH_3CH(NO_3)CH(C_3H_7)O^\bullet$ (MCM notation: C62NO33O), formed in the $NO_3$-oxidation scheme of trans-2-hexene, the decomposition reaction rate should likely be adjusted by a similar amount. However, its dominant loss is isomerisation by H-migration, such that we are not sensitive to the rate coefficient for decomposition for this compound.

# D Instrumentation details

Table S2: Instrumentation for radical and trace-gas measurements during the presented experiments.

| Species | Technique | Time resolution | 1 σ precision | 1 σ accuracy |
|---|---|---|---|---|
| OH | LIF | 45 s | $2.8 \times 10^5$ cm$^-$3 | 18 % |
| $HO_2$ | LIF | 45 s | $2.9 \times 10^7$ cm$^-$3 | 18 % |
| $RO_2$ | LIF | 45 s | $5.6 \times 10^7$ cm$^-$3 | 18 % |
| $k_{OH}$ | Laser photolysis+LIF | 132 s | 0.4 s$^-$1 | 10 % |
| $O_3$ | UV absorption | 60 s | 1 ppbv | 5 % |
| CO | CRDS | 60 s | 1.5 ppbv | 1 % |
| Acetaldehyde | PTR-TOF-MS | 30 s | >15 pptv | 10 % |
| NO | Chemiluminescence | 45 s | 10 pptv | 5 % |
| $NO_2$ | Chemiluminescence | 97 s | 2 pptv | 5 % |

# E Contribution of $NO_3$ and $O_3$ to the oxidation of cis-2-butene and trans-2-hexene

Table S3: Overview of performed cis-2-butene and trans-2-hexene experiments. The contributions of ozonolysis and reaction with $NO_3$ to the oxidation of the VOCs are listed.

| Temperature [K] | Experimental description | Contribution $O_3$ [%] | Contribution $NO_3$ [%] |
|---|---|---|---|
| Cis-2-butene | | | |
| 295 | CO addition | 54 | 46 |
| 276 | CO addition | 38 | 63 |
| Trans-2-hexene | | | |
| 305 | CO addition | 14 | 86 |
| 292 | CO addition | 22 | 78 |
| 279 | $CH_4$ addition | 46 | 54 |
| 276 | CO addition | 45 | 55 |

# F Comparison of modelled and measured acetaldehyde from the oxidation of cis-2-butene by $NO_3$

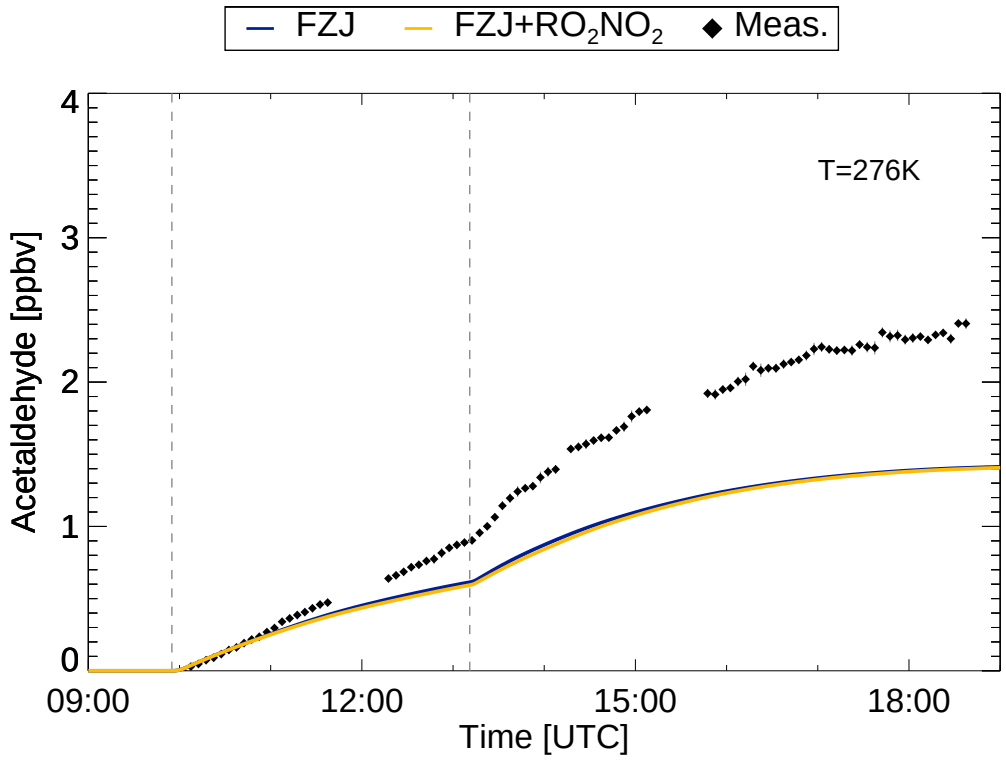


Figure S11: Comparison of modelled and measured (5 minutes average) acetaldehyde in the nighttime experiments of cis-2-butene at cold conditions. Model results displayed as FZJ (blue) and FZJ+$RO_2NO_2$ (brown) models refer to the FZJ mechanism without and with the additional formation of non-acyl $RO_2NO_2$, respectively. Injections of chemical species into the chamber are marked by vertical lines.

# G Nighttime oxidation of trans-2-hexene at different temperatures

Experiments focussing on the nighttime oxidation of trans-2-hexene were performed at three different temperatures: at cold temperatures of $\sim 276$ K (Fig. 2) and $\sim 279$ K (Fig. 3), and at medium ($T \approx 292$ K) and hot ($T \approx 305$ K) temperatures (Fig. S12). In the main paper, the experiment conducted at $T \approx 276$ K was already presented. Here, we discuss the experiments at medium and hot temperatures, and compare them to the experiment performed at cold temperatures.

For hot conditions, the FZJ mechanisms, with and without additional $RO_2NO_2$ formation,

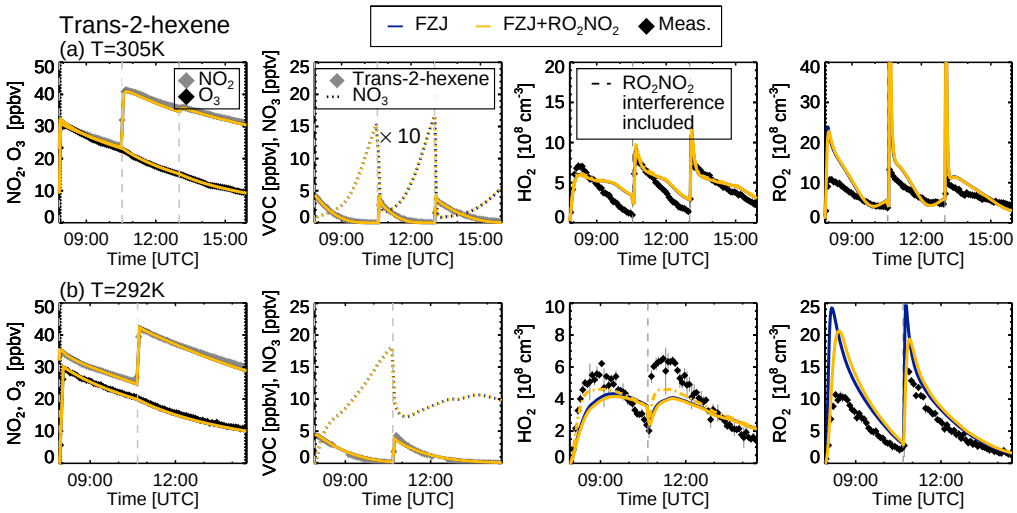


Figure S12: Comparison between modelled and measured (5 minutes average) trace gases and $HO_2$ and $RO_2$ radical concentrations in the trans-2-hexene experiments with CO as OH scavenger. Model results displayed as FZJ (blue) and FZJ+$RO_2NO_2$ (brown) models refer to the FZJ mechanism with and without the additional formation of non-acyl $RO_2NO_2$, respectively. For the experiment conducted at 305 K, the formation of $HNO_2$ was considered according to Eq. (S4). Injections of chemical species into the chamber are marked by vertical lines.

overestimate the measured $RO_2$ radical concentration by a factor of up to 1.5, after 0.5 h after the VOC was (re-)injected. Directly after the VOC injections, especially after the second and third injection, a very large peak concentration of $RO_2$ (up to $6 \times 10^9$ cm$^{-3}$) is predicted by all mechanisms which is not observed in the measurements. Since trans-2-hexene was completely consumed before it was re-injected the second or third time, the mechanisms predict $NO_3$ concentrations to build up, reaching up to 150 pptv. The high $NO_3$ concentration then reacts rapidly with the newly injected trans-2-hexene, generating the very large concentration of modelled $RO_2$ radicals until a new equilibrium between $NO_3$ and $N_2O_5$ is reached. However, these large $RO_2$ radical concentrations are not observed, suggesting unknown chamber reactions for $NO_3$ when trans-2-hexene is not dominating, which cannot be described correctly in the presented experiments due to missing $NO_3$ and $N_2O_5$ measurements.

In the experiment at medium temperatures, the FZJ mechanisms overestimate the measured $RO_2$ radical concentrations on average by a factor of 1.5, where the FZJ+$RO_2NO_2$ model, including non-acyl $RO_2NO_2$ formation, predicts a time-dependence that better

agrees with the observations.

The agreement between measured and modelled $HO_2$ radical concentrations differs significantly in the experiments at the three temperatures. At low temperatures (cold), the measured $HO_2$ is highly underestimated by a factor of 3. The underestimation is only a factor of 1.1 in the experiment at medium temperatures. In the experiment at high temperatures (hot), an overestimation of the detected $HO_2$ is observed with an average model-to-measurement ratio of 1.4.

At higher temperatures, the isomerisation of $RO_2$ radicals, with rates derived from the SAR from Vereecken and Nozière[5], increasingly contributes to the $HO_2$ production rate (from 23 % for cold to 34 % for hot conditions) and thus leads to higher $HO_2$ radical concentrations. Through the reaction of $HO_2$ with $RO_2$, the $HO_2$ radical can be recycled by forming OH which will subsequently react with CO producing $HO_2$ again. Therefore, it is difficult to understand why the measured $HO_2$ radical concentrations in the experiment at cold conditions are so similar as in the experiment at medium temperatures when the source strength should have increased substantially at a similar $HO_2$ loss rate. In contrast to the $NO_3$ experiment performed at cold conditions, a good agreement between modelled and measured $HO_2$ is observed in the ozonolysis experiment, which was performed at cold conditions as well (Fig. S2, Section E.2). Therefore, the observed model-measurement discrepancy in the $HO_2$ radical concentrations is unlikely to be caused by the oxidation of trans-2-hexene by $O_3$ and, thus, arises either from the contribution of the oxidation of trans-2-hexene by $NO_3$ or by the presence of $NO_2$.

The amount of $RO_2NO_2$ reservoir species formed in the experiments with trans-2-hexene

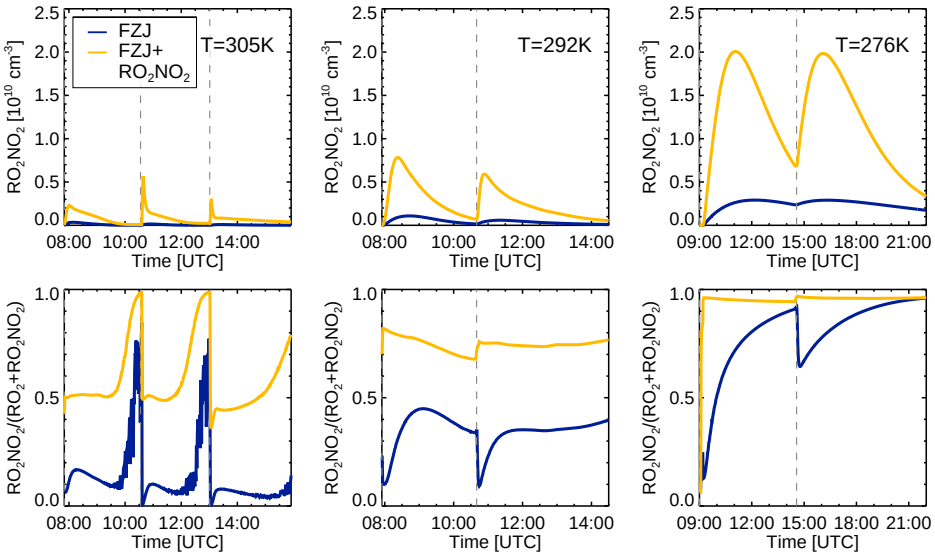


Figure S13: Formed non-acyl $RO_2NO_2$ concentrations and the fraction of non-acyl $RO_2$ stored as $RO_2NO_2$ ($RO_2NO_2/(RO_2+RO_2NO_2)$) for the three trans-2-hexene oxidation experiments in the presence of $NO_2$ applying the FZJ mechanism either without (FZJ model, blue) or with (FZJ+$RO_2NO_2$ model, brown) the additional formation of alkyl-$RO_2NO_2$. Model results of the $RO_2NO_2$ concentrations, based on the FZJ mechanism without additional formation of $RO_2NO_2$ (FZJ model), refer to $CH_3O_2NO_2$ concentrations. Vertical lines refer to the injection of chemical species.

at the different tested temperatures is shown in Fig. S13, together with the fraction of non-acyl $RO_2$ radicals stored as $RO_2NO_2$. $RO_2NO_2$ mixing ratios are predicted to increase from 100 pptv to up to 750 pptv over a temperature range of 305 K to 276 K, resulting in 50 % to 95 % less non-acyl $RO_2$ radicals, respectively. The impact of this high amount of non-acyl $RO_2$ radicals stored as $RO_2NO_2$ reservoir species is discussed in Sections 3.2

and 4 in the main paper.

Concentrations of acetaldehyde observed in the experiments with trans-2-hexene are shown in Fig. S14. The comparison between measured and modelled acetaldehyde is discussed in Section 3.2 in the main paper.

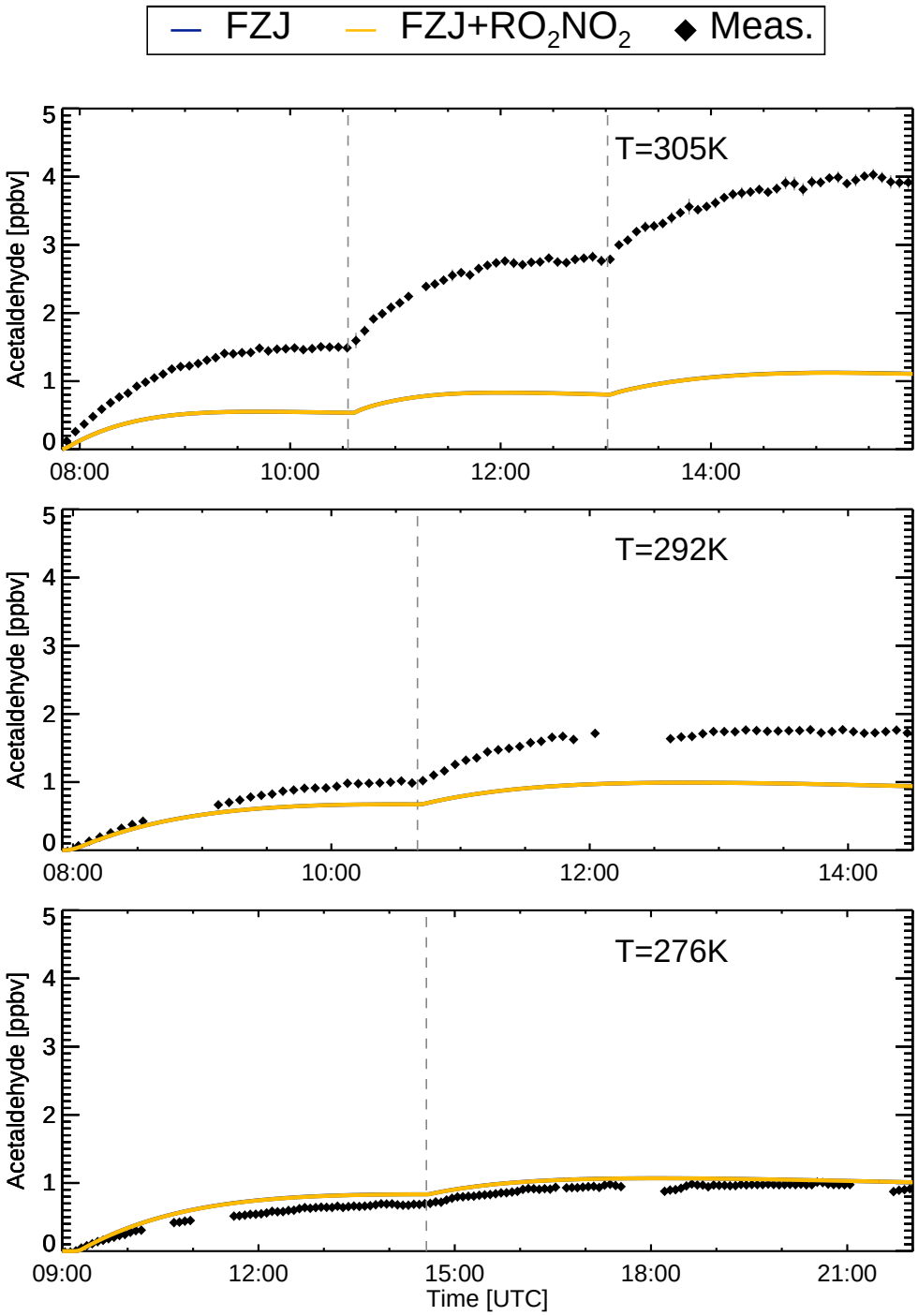


Figure S14: Comparison of modelled and measured (5 minutes average) acetaldehyde in the trans-2-hexene $NO_3$ experiments. Model results displayed as FZJ (blue) and FZJ+$RO_2NO_2$ (brown) models refer to the FZJ mechanism without and with the additional formation of non-acyl $RO_2NO_2$, respectively. Injections of chemical species into the chamber are marked by vertical lines.

## G.1 Overestimation of $HO_2$ radical concentrations observed for hot conditions

For hot conditions, an overestimation of the measured $HO_2$ radical concentration by both, the FZJ and FZJ+$RO_2NO_2$ mechanisms, is observed. The discrepancy could be improved by accounting for the formation of nitryl hydride ($HNO_2$) from the reaction of $HO_2$ with $NO_2$[6]:

$$HO_2 + NO_2 \rightarrow HNO_2 + O_2, \tag{S4}$$

which rate coefficient can be described by the following Arrhenius expression: $k_{Eq.\ (S4)} = 1 \times 10^{-10} \times \exp(-(27.4 \pm 0.4)\,\mathrm{kJ\,mol^{-1}}/(RT))$[6]. Reactions of nitryl hydride are typically investigated at temperatures relevant in combustion processes, *i.e.* temperatures much larger than 305 K. At these temperatures, $HNO_2$ was observed to undergo bimolecular reactions with a number of radicals such as the hydrogen atom or the methyl radical[7–10]. Also unimolecular reactions forming HONO or OH + NO were studied[9–11], which were found to not impact the model results at the given temperatures. Including the formation of $HNO_2$ improves the model-measurement agreement for $HO_2$ by $\sim 30\,\%$ leading to an agreement within $\sim 30\,\%$.

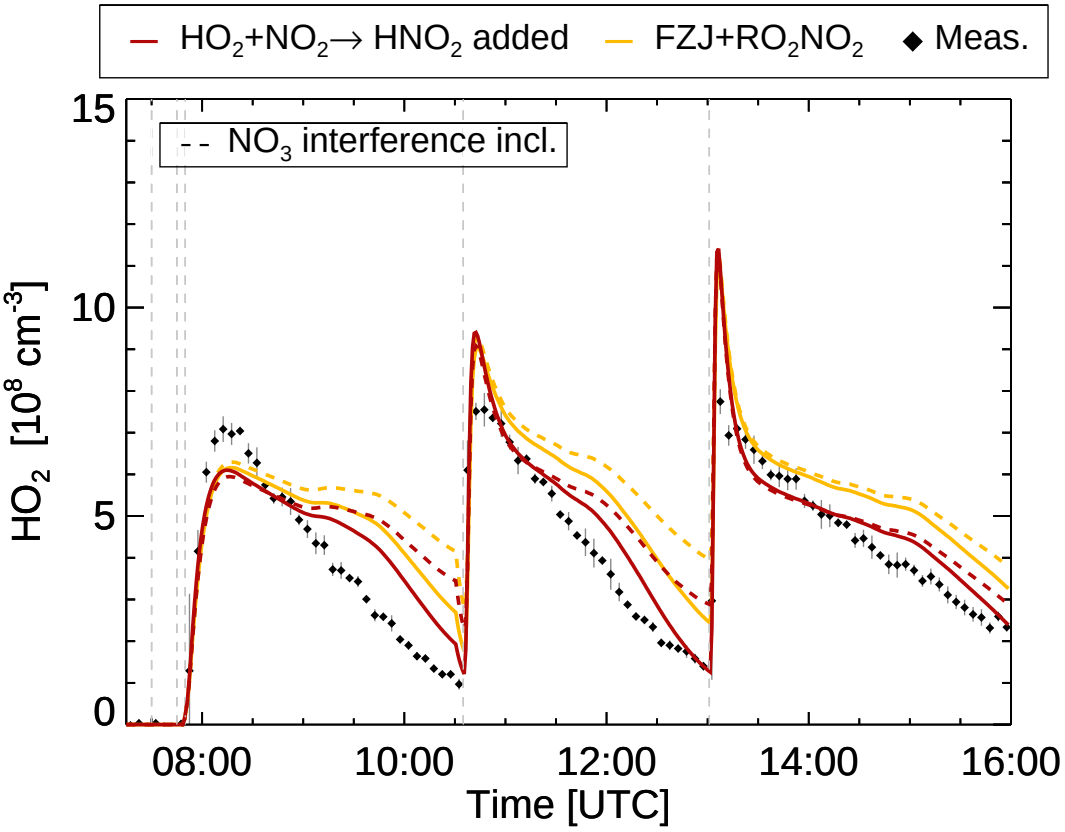


Figure S15: Modelled and measured (5 minutes average) $HO_2$ radical concentrations for the FZJ mechanism including additional formation of non-acyl $RO_2NO_2$ (FZJ+$RO_2NO_2$ model), with and without the formation of $HNO_2$ from the reaction of $HO_2$ with $NO_2$. Injections of chemical species into the chamber are marked by vertical lines.

## G.2 Further analysis of the remaining uncertainties

Measured values of acetaldehyde are well reproduced in the experiment with trans-2-hexene at cold conditions but are underestimated by the FZJ mechanisms in the experiments at medium and hot conditions (Fig. S14). In both FZJ mechanisms, acetaldehyde is mainly produced (> 93 %) directly from the ozonolysis of trans-2-hexene and is lost via dilution. An erroneous rate constant of the ozonolysis reaction is unlikely to be the reason for the observed model-measurement differences since the time series of trans-2-hexene is well reproduced at all probed temperatures. Therefore, it is likely that the yield of acetaldehyde in the chemical mechanism is too small or, given that a good model-measurement agreement is found at the low temperatures, that the temperature-dependence of the yield is incorrect. Indeed, the updated ozonolysis scheme in Novelli *et al.*[1] as well as the ozonolysis SAR from Newland *et al.*[2] do not provide temperature-dependent product yields, and further experiments at higher temperatures would be useful to improve the product yields.

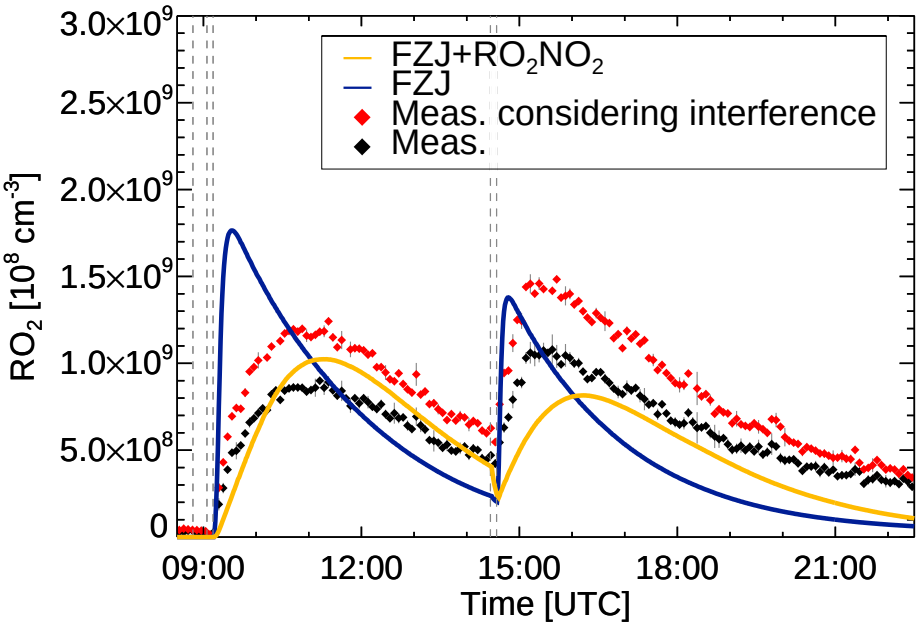


Figure S16: Comparison of the time series of $RO_2$ radical concentrations with and without considering a possible interference in the $HO_x$ measurement in the trans-2-hexene experiment with CO as OH scavenger at 276 K. Model results from the FZJ mechanism with (FZJ+$RO_2NO_2$ model, brown) and without (FZJ model, blue) the additional formation of non-acyl $RO_2NO_2$ are shown as well. Injections of chemical species into the chamber are marked by vertical lines.

# References


[1] A. Novelli, C. Cho, H. Fuchs, A. Hofzumahaus, F. Rohrer, R. Tillmann, A. Kiendler-Scharr, A. Wahner and L. Vereecken, *Phys. Chem. Chem. Phys.*, 2021, **23**, 5474–5495.

[2] M. J. Newland, C. Mouchel-Vallon, R. Valorso, B. Aumont, L. Vereecken, M. E. Jenkin and A. R. Rickard, *Atmos. Chem. Phys.*, 2022, **22**, 6167–6195.

[3] M. E. Jenkin, R. Valorso, B. Aumont and A. R. Rickard, *Atmos. Chem. Phys.*, 2019, **19**, 7691–7717.

[4] H. Fuchs, Z. Tan, A. Hofzumahaus, S. Broch, H.-P. Dorn, F. Holland, C. Künstler, S. Gomm, F. Rohrer, S. Schrade, R. Tillmann and A. Wahner, *Atmos. Meas. Tech.*, 2016, **9**, 1431–1447.

[5] L. Vereecken and B. Nozière, *Atmos. Chem. Phys.*, 2020, **20**, 7429–7458.

[6] K. McKee, M. A. Blitz, R. J. Shannon and M. J. Pilling, *J. Phys. Chem. A*, 2022, **126**, 7514–7522.

[7] M. E. Fuller and C. F. Goldsmith, *Proc. Combust. Inst.*, 2019, **37**, 695–702.

[8] O. Mathieu, B. Giri, A. Agard, T. Adams, J. Mertens and E. Petersen, *Fuel*, 2016, **182**, 597–612.

[9] Y. Zhang, O. Mathieu, E. L. Petersen, G. Bourque and H. J. Curran, *Combust. Flame*, 2017, **182**, 122–141.

[10] S. F. Ahmed, J. Santner, F. L. Dryer, B. Padak and T. I. Farouk, *Energy Fuels*, 2016, **30**, 7691–7703.

[11] X. Chen, M. E. Fuller and C. Franklin Goldsmith, *React. Chem. Eng.*, 2019, **4**, 323–333.